Seismicity overview of the Mohns Ridge and Knipovich Ridge 1955-2015

Víkingur Logi Ásgeirsson

Faculty of Geoscience
University of Iceland
2015

SEISMICITY OVERVIEW OF THE MOHNS RIDGE AND KNIPOVICH RIDGE 1955-2015

Víkingur Logi Ásgeirsson

10 ECTS thesis submitted in partial fulfillment of a
Baccalaureum Scientiarum degree in Geophysics

Advisor
Páll Einarsson

Faculty of Geoscience
School of Engineering and Natural Sciences
University of Iceland
Reykjavik, October 2015

Seismicity overview of the Mohns Ridge and Knipovich Ridge 1955-2015
Mohns and Knipovich seismicity
10 ECTS thesis submitted in partial fulfillment of a B.Sc. degree in Geophysics

Faculty of Geoscience
School of Engineering and Natural Sciences
University of Iceland
Iceland

Bibliographic information:
Víkingur Logi Ásgeirsson, 2015, Seismicity overview of the Mohns Ridge and Knipovich Ridge 1955-2015, B.Sc. thesis, Faculty of Geoscience, University of Iceland.

Printing: Háskólaprent, Fálkagata 2, 107 Reykjavík
Reykjavik, Iceland, October 2015

Abstract

This thesis gives an overview of seismic activity on the Mohns and Knipovich ridges for the period of 1955-2015. Fault plane solutions on both ridges are dominated by normal faulting trending with the ridge axes. The Mohns Ridge is quite active and its seismicity is similar to that of large parts of the Mid-Atlantic Ridge, with earthquakes concentrated near the ridge's axis. The Knipovich Ridge is less active and shows less typical characteristics; seismic activity is not concentrated on the axis but is rather diffuse. One segment of the Knipovich Ridge shows anomalously high seismicity. The Jan Mayen Fracture Zone is very active seismically and normal, reverse, and strike-slip faulting is present. The Molløy Fracture Zone is not very active and strike-slip and normal faulting is present. Where each ridge connects to its respective fracture zone, there is a 20-30 km band of very little earthquake activity. Several large earthquakes were present in the data, the largest six of which ($M_W \geq 6.0$) took place on the fracture zones and the Mohns Ridge. Few noteworthy earthquake swarms were observed. Intraplate earthquakes were mostly small and concentrated to the east of the ridges. Gutenberg-Richter b-values were calculated for each ridge, with the Mohns Ridge values ranging between 1.61 and 1.81 and Knipovich Ridge values ranging between 1.57 and 1.75. The Mohns Ridge showed no clear trend regarding the seismic moment, while the Knipovich Ridge shows a downward trend towards the north, aside from the one very active ridge segment near 76.35°N. The Jan Mayen Fracture Zone showed the highest normalized seismic moment of any segment in the area, while the Molløy Fracture Zone was among the lowest. Calculated ridge spreading rate and azimuth ranges from 14.38 mm/yr, 128.3° at the northern end of the Knipovich Ridge to 16.91 mm/yr, 114.7° at the southern end of the Mohns Ridge.

Útdráttur

Þessi ritgerð veitir yfirlit yfir jarðskjálftavirkni á Mohns og Knipovich hryggjum á tímabilinu 1955-2015. Brotlausnir á báðum hryggjum einkennast af siggengislausnum með hreyfingu þvert á ása hryggjanna. Mohns hryggur er nokkuð virkur og skjálftavirkni á honum svipar til virkninnar á stórum hluta mið-Atlantshafshryggjarins, skjáftarnir eiga sér stað nálægt ás hryggjarins. Knipovich hryggur er ekki jafnvirkur og er virkni hans óvenjulegri; jarðskjálftar safnast ekki saman við ásinn heldur dreifast þeir yfir stærra svæði. Einn bútur Knipovich hryggjar sýnir óvenjuháa skjálftavirkni. Jan Mayen þverbrotabeltið einkennist af mjög mikilli jarðskjálftavirkni og siggengis-, samgengis- og þvergengisbrotlausnir eru til staðar á því. Molløy þverbrotabeltið sýnir ekki mikla virkni, en þar eru sniðgengis- og siggengisbrotlausnir til staðar. Á þeim stöðum þar sem hryggirnir tveir tengjast sínum þverbrotabeltum virðist vera 20-30 km svæði þar sem skjálftavirkni er afar lítil. Þónokkrir stórir skjálftar fundust í gögnunum, en þeir sex stærstu ($M_W \geq 6.0$) áttu sér stað á þverbrotabeltunum og Mohns hrygg. Fáar greinilegar skjálftahrinur fundust. Innflekaskjálftar voru að mestu leyti smáir og áttu sér stað austan megin hryggjanna. Gutenberg-Richter b-gildi voru reiknuð út fyrir hryggina tvo. Gildin á Mohns-hrygg voru á bilinu 1.61-1.81 og á Knipovich hrygg voru þau á bilinu 1.57-1.75. Skjálftavægi á Mohns hrygg sýnir enga sérstaka hneigð, en á Knipovich hrygg minnkar skjálftavægið til norðurs, nema á einu stykki hans nálægt 76.35°N. Jan Mayen þverbrotabeltið hefur hæsta staðlaða skjálftavægið á svæðinu, en vægið á Molløy þverbrotabeltinu er með því lægsta sem sást. Reiknuð gildi rekhraða og -stefnu eru frá 14.38 mm/ári, 128.3° við norðurenda Knipovich hryggjar og til 16.91 mm/ári, 114.7° við suðurenda Mohns hryggjar.

Contents

List of Figures

List of Tables

Acknowledgments

Firstly, I would like to thank my parents for without them I would not exist. I would also like to thank my whole family for supporting me while writing this thesis. Special thanks to my advisor Páll Einarsson for his guidance and willingness to assist me in answering the many questions that came up during this project.

1 Introduction

The Mid-Atlantic Ridge is an oceanic ridge that follows the North-South axis of the Atlantic Ocean. The southern part of the ridge separates the African and South American tectonic plates, while the northern part separates the Eurasian and North American plates. The Arctic Ridge system extends northward from the Mid-Atlantic Ridge and consists of four ridges, the Kolbeinsey, Mohns, Knipovich and Gakkel ridges. The Mohns Ridge is bounded by the Jan Mayen Fracture Zone in the South and the Knipovich Ridge in the north. The Knipovich Ridge then extends further north to the Molløy Fracture Zone near Svalbard. As with any divergent plate boundary, earthquakes are frequent on these ridges and this seismic activity has been continuously monitored for more than the sixty years by various agencies and institutions around the world.
The aim of this thesis is to give a general overview of the earthquake activity on the Mohns and Knipovich ridges by examining sixty years of seismological data provided by the ISC. Focal mechanisms and seismic events will be mapped, and a frequency-magnitude distribution will be calculated for each ridge. Major tectonic events, such as large earthquakes and earthquake swarms will be described, followed by a calculation of the total seismic moment for the various ridge segments. Additionally, the seafloor spreading rate will be calculated at each earthquake location with the NUVEL 1a model and compared to current measurements of spreading rates.

2 Regional background

2.1 Mohns Ridge

The Arctic Mid-ocean Ridge system extends northward from the Mid-Atlantic Ridge. This system began opening approximately 53 Ma ago, splitting the Lomonosov Ridge and Greenland from the Eurasian plate. The Mohns Ridge extends from the Jan Mayen Fracture Zone at around 71.15°N to the Knipovich Ridge at 73.9°. The ridge is over 500 km long and it follows a N60° trend. Magnetic data reveal that the spreading direction of the Mohns Ridge appears to have changed from NNW-SSE to NW-SE around 25 Ma (Okino et al., 2002). The current spreading direction of the ridge is 110°N, close to the trend of the Jan Mayen Fracture Zone. In general, oceanic spreading is often perpendicular to the ridge axis (90° between ridge axis and spreading direction), but in this case it is clear that the spreading direction is highly oblique to the trend, the angle between the two being 40° to 50°. The ridge's axial valley is continuous and its width ranges from 8-15 km. The rift valley shoulders are heavily asymmetric, with the northwest shoulder being made up of slopes of variable trends and the southeast shoulder having a smoother topography with slopes parallel to the axial trend. The mean depth of the ridge valley decreases in the southwest, due to proximity to the Icelandic hotspot (Dauteuil & Brun, 1996). Earthquakes on the ridge mostly occur along a well defined seismic zone, which is narrow and continuously follows the rifted crest. The seismicity is comparable to other parts of the Mid-Atlantic Ridge, but considerably higher than that of the Kolbeinsey Ridge and northern Reykjanes Ridge, possibly due to the influence of the Icelandic hotspot on the brittle-ductile boundary. Previous fault plane solutions have shown that normal faulting dominates on the ridge axis (Einarsson, 1986). The pattern of seismicity changes abruptly once the Mohns Ridge meets the Knipovich Ridge.

2.2 Knipovich Ridge

The Knipovich Ridge stretches from its junction with the Mohns Ridge at 73.9°N to the northwest for around 500 km to the Molløy Fracture Zone at about 78.5°.

Not much is known about the spreading history of the Knipovich Ridge, because no clear magnetic anomaly pattern exists around the ridge. It has been suggested that the Knipovich Ridge originated as a shear-zone or continental transform that linked the Gakkel and Mohns ridges early in the history of the Arctic Ridge system. This transform then evolved into a spreading center at a later time (Okino et al., 2002). The western flank of the Knipovich Ridge area is more elevated than the eastern flank (by several hundred meters), likely due to a heavy sedimentation load on the eastern side, primarily deposited by the Svalbard archipelago and the Barents Sea shelf.
The ridge has been classified as an ultra-slow spreading ridge and the direction of spreading is highly oblique to the plate boundary. Magnetic anomalies on the ridge display an anomalous, diffuse pattern, with proposed explanations such as thermal blanketing from the thick sedimentary load on the eastern side, a wide zone of magma injection, or fragmentation due to axial shifts (Kandilarov, Mjelde, Okino, & Murai, 2008). This unusual magnetic pattern prevents estimation of the spreading rate by magnetic data, and so thermal modeling is used instead, which is a less reliable method. The spreading on the ridge is highly asymmetric, with a rate of only 1 mm/yr to the east and 7 mm/yr to the west. Seismicity on the ridge appears to be much more diffuse than on most other ridges, and scattered earthquake epicenters imply that deformation takes place over a wide area (Einarsson, 1986).

3 Fault plane solutions

A focal mechanism or fault plane solution is a graphical representation of the deformation that occurs at the hypocenter of a seismic event and it tells us the orientation of the two possible fault planes that could have produced the recorded seismic waveforms. A common method for determining a focal mechanism is to analyze the first motion of the body-or surface waves from an earthquake, with the simplest form analyzing P-waves arrivals. P-waves radiate from the hypocenter with compressional or dilatational(tensional) initial motion. On a vertical seismogram, a compression is recorded as an upward movement and a dilatation is recorded as a downward motion, while observations made close to the nodal plane often yield no clear first motion. With a reasonably distributed net of seismograph stations around an earthquake, it is then possible to determine which regions experience compression and tension. The first motions of the P-waves are then plotted onto a lower-hemisphere stereographic projection, with filled circles representing stations that record compression and empty circles for stations that record dilatation, see figure 3.1. One can then draw two orthogonal great circles that divide the compressive from the tensional motion, these represent the two nodal planes for the faulting (Cronin, 2004). The compressional quadrants are then colored in, and the tensional quadrants are left blank, creating a beach ball diagram.
Another method for determining the focal mechanism is through the use of a moment tensor solution, which also utilizes the radiation pattern of waves from an event. However, it uses the complete waveform data to better determine the radiation pattern, see figure 3.2 (Barth, Reinecker, & Heidbach, 2008). The axis of maximum shortening is known as the P axis and lies within the dilatational quadrants while the axis of maximum lengthening, the T axis, lies within the compressional quadrants. The axis formed by the intersection of these two is the null or B axis.

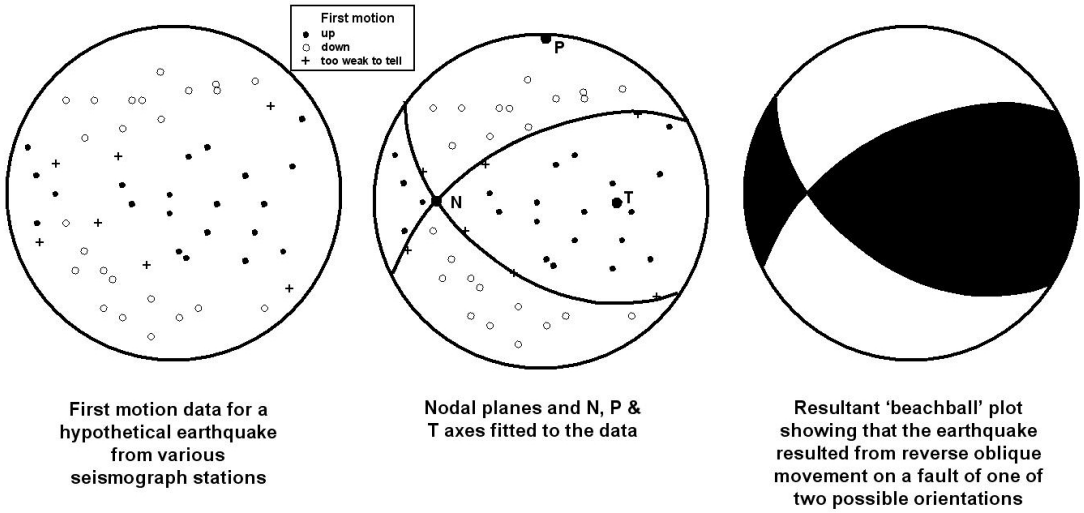

Figure 3.1: Using P-wave first arrivals to construct beach-ball diagram (Norton, 2008b).

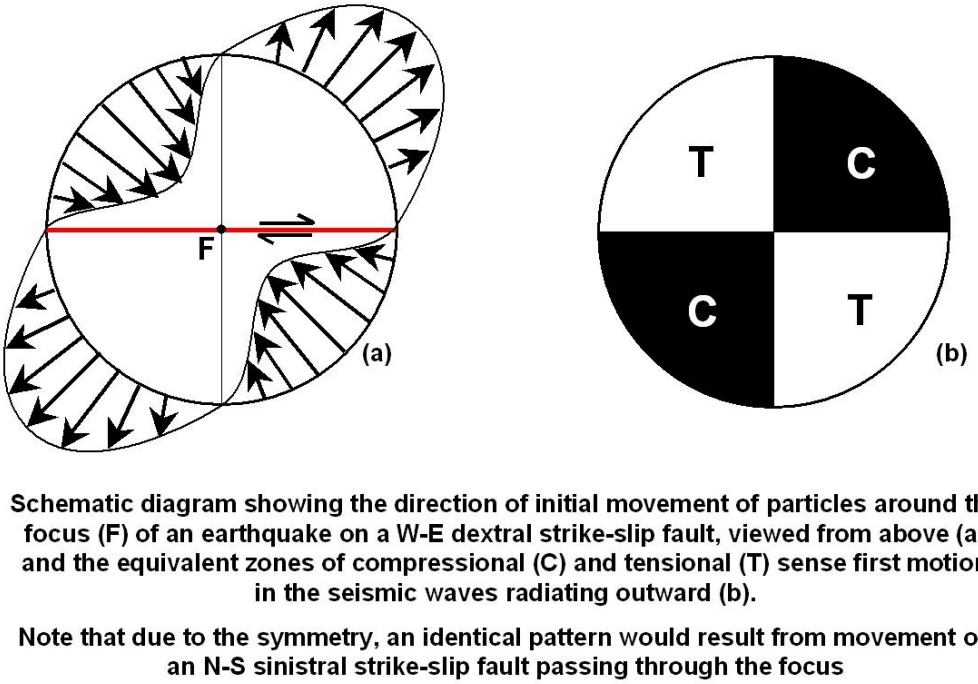

Figure 3.2: Moment tensors used to construct beach-ball diagram (Norton, 2008a)

The beach-ball diagrams give us the two possible nodal planes for a faulting event,

and in order to distinguish the (actual) fault plane from the auxiliary plane, we need additional geological knowledge of the area around the earthquake.
The beach-ball diagram tells us whether the fault responsible was a normal, reverse, strike-slip, or a combination of two of these. This information in turn lets us make an educated guess as to what happened at the earthquake hypocenter (Cronin, 2004). During normal faulting, the block above the fault moves downward relative to the block above the fault. During reverse faulting, the block above the fault moves up, relative to the block below the fault. During a strike-slip event, the movement of blocks along the fault is horizontal, and can be right-or left-lateral. Oblique faulting is a combination of either strike-slip and normal faulting or strike-slip and reverse faulting. On divergent plate boundaries, normal faulting is the most common, since there are two plates or blocks moving away from one another at the fault. Transform fracture zones are mostly characterized by strike-slip faulting.

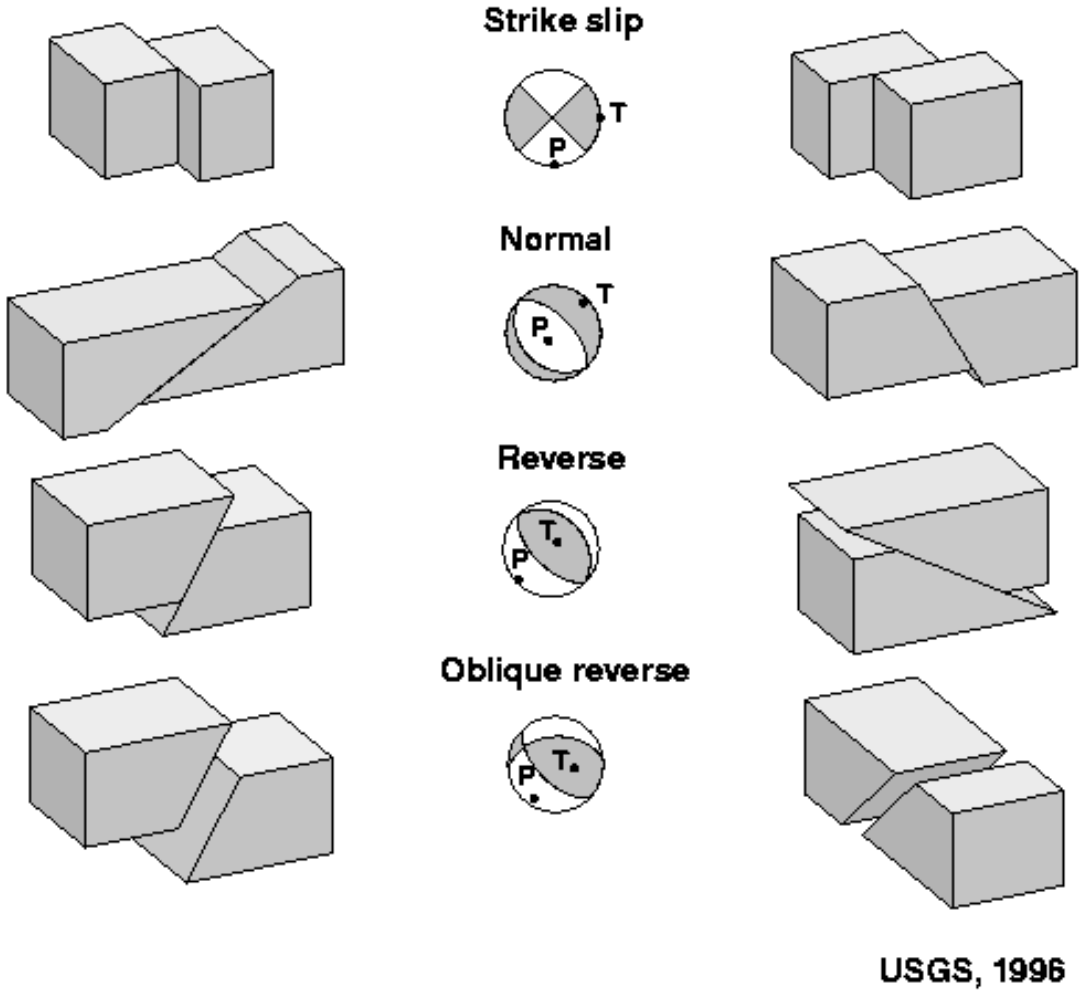

Figure 3.3: For each beach-ball there are two possible fault planes (USGS, 1996).

In some seismic events, there is simultaneous vertical extension and horizontal compression or vice-versa. These are known as non double-couple components and may accompany the other types of movement. Beach-ball diagrams that contain both types of motion will often resemble a fried egg.
Complete data on all fault plane solutions in this project may be found in Appendix A.

4 Data

All of the data used for this project have been collected from the International Seismological Center's bulletin search (ISC, 2015). These are teleseismic measurements from various agencies around the world collated by the ISC. For each seismic event, the available prime hypocenter data were used. The data not listed for the prime hypocenter were obtained from any of the other available sources, with the most trustworthy (somewhat arbitrarily ranked) agencies being preferred. The search parameters used are shown in the table below:

Table 4.1: Search parameters

Bottom latitude	70.8
Top latitude	78.7
Left longitude	-9.66
Right longitude	15
Start date	01/01/1955
End date	13/3/2015
Min magnitude	4.0

A total of 1341 seismic events matched the search parameters, but some of these were not used during processing, due to missing or very low (< 4.0) m_b and M_S values. The data were output in an XML format and then input into Microsoft Excel 2013. The bulk of the processing was done using Excel. The magnitude values of interest here are the body wave magnitude m_b, surface wave magnitude M_S and moment magnitude M_W. Both the m_b and M_S scales are useful for characterizing earthquakes of a magnitude up to 5.5, at which point they begin to saturate, i.e. giving lower values than anticipated. For these larger events, the moment magnitude scale M_W is generally used. M_W measurements are usually only available for large earthquakes with computed fault plane solutions (Fowler, 1990).

5 Discussion

5.1 Mapping

Mapping was done using Esri's ArcMap software. The bathymetric map was downloaded from the GEBCO website (GEBCO, n.d.). A few different maps were produced in order to paint a clearer picture of the seismic activity in the region. Each ridge was split into ten segments by latitude, which are displayed on the overview maps (see Appendix B for coordinates). The overview map (figure 5.1) shows every event with a magnitude $m_b \geq 4.0$ that took place in the area between 1/1/1955 and 15/3/2015. This map was further separated into two maps, one for each ridge. The dominant fault plane solution for each region is displayed along the border of each map. Separate maps were made for the fracture zones as well, displaying every available fault plane solution.

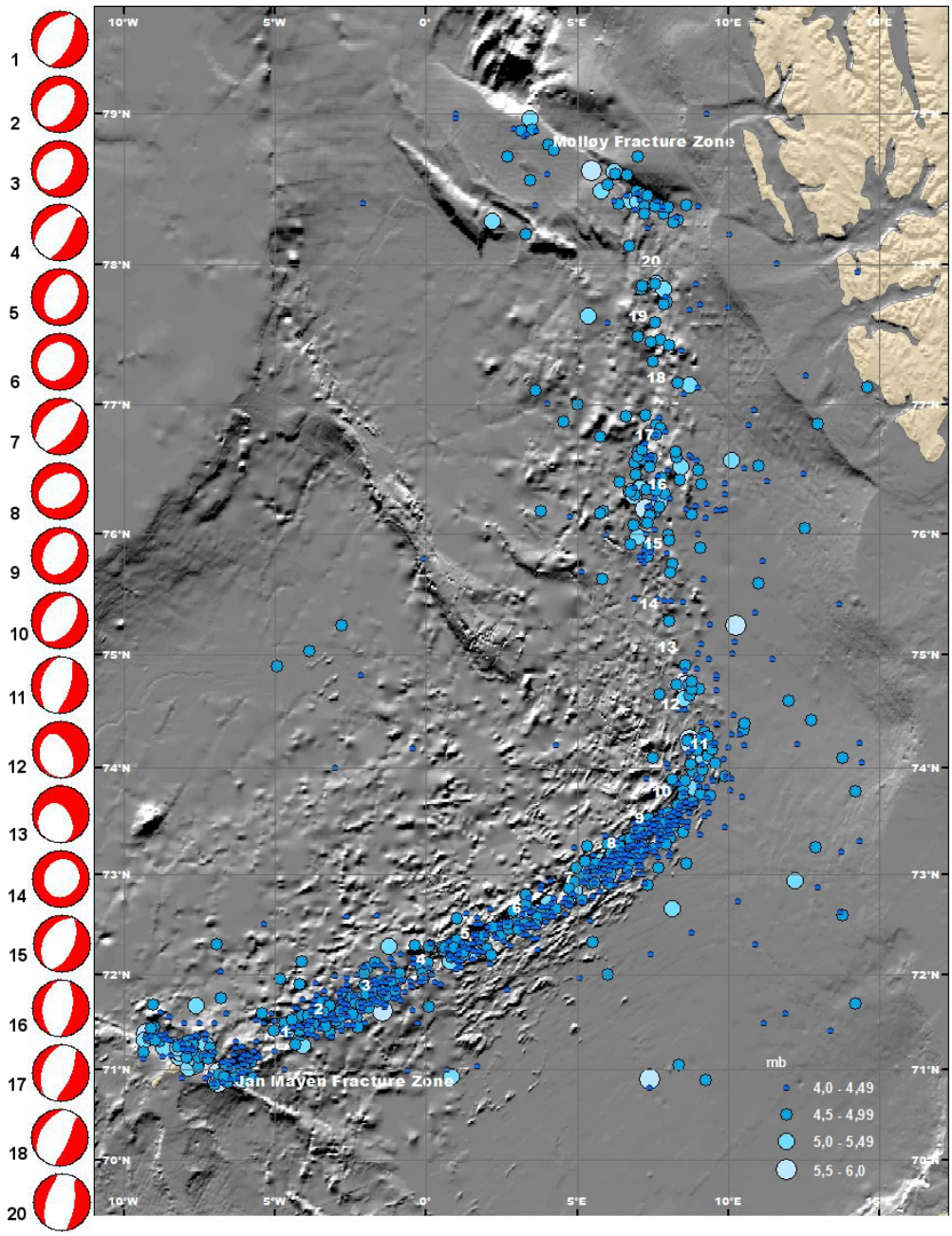

Figure 5.1: Overview map showing earthquake epicenters for all events with $m_b \geq 4.0$ around the Mohns and Knipovich Ridges. Data were obtained from the International Seismological Centre's bulletin. Bathymetric map obtained from GEBCO. Map uses Mercator projection.

A total of 1069 earthquake epicenters are displayed on the overview map. The difference in seismicity between the Mohns Ridge and Knipovich Ridge is readily apparent. The former shows greater activity than the latter. Earthquake epicenters

are confined to an area close to the axis of the Mohns Ridge, whereas activity on the Knipovich Ridge is very diffuse and it can be difficult to infer the position of the ridge axis from the epicenter data alone. Intraplate earthquake activity is more prevalent to the east of the ridges than the west, with several large quakes visible in the eastern part but only a handful of small/midsized quakes in the western part.

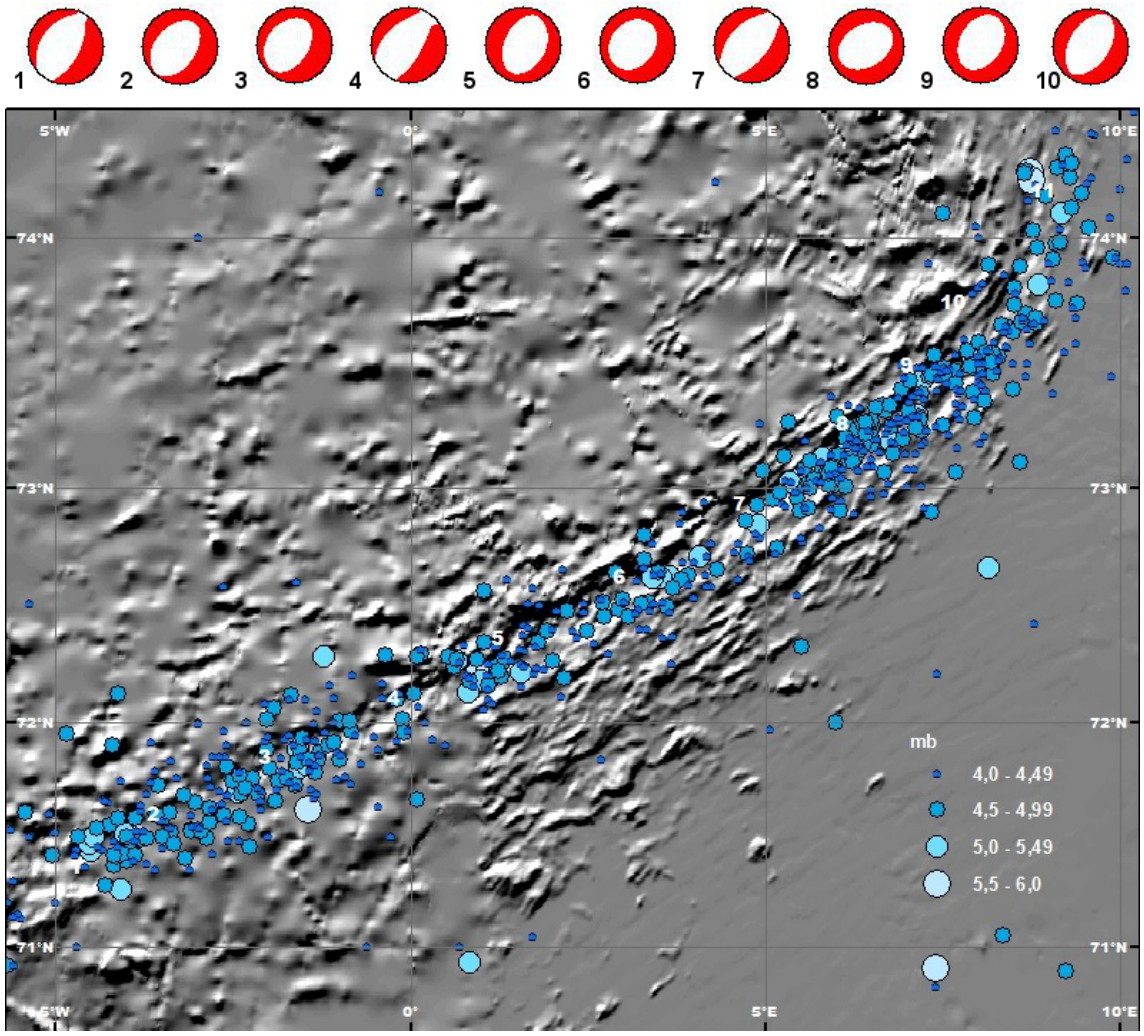

Figure 5.2: Overview map showing earthquake epicenters for all events with $m_b \geq 4.0$ around the Mohns Ridge. Data were obtained from the International Seismological Centre's bulletin. Bathymetric map obtained from GEBCO. Map uses Mercator projection.

When we zoom in on the Mohns Ridge, we see that earthquake activity on it is quite well constrained to the ridge axis. The activity shows no clear trends or breaks, being relatively evenly distributed over the whole ridge. There is a clear zone of low activity where the ridge meets the Jan Mayen Fracture Zone, seen on

the lower left. Every one of the ten fault plane FPSs for the ridge shows normal faulting with a trend close to the axis. More than half of them show a non-double-couple component, indicating a change in volume at the hypocenter. These fault mechanisms are typical for a spreading ridge, none of them are anomalous for this area.

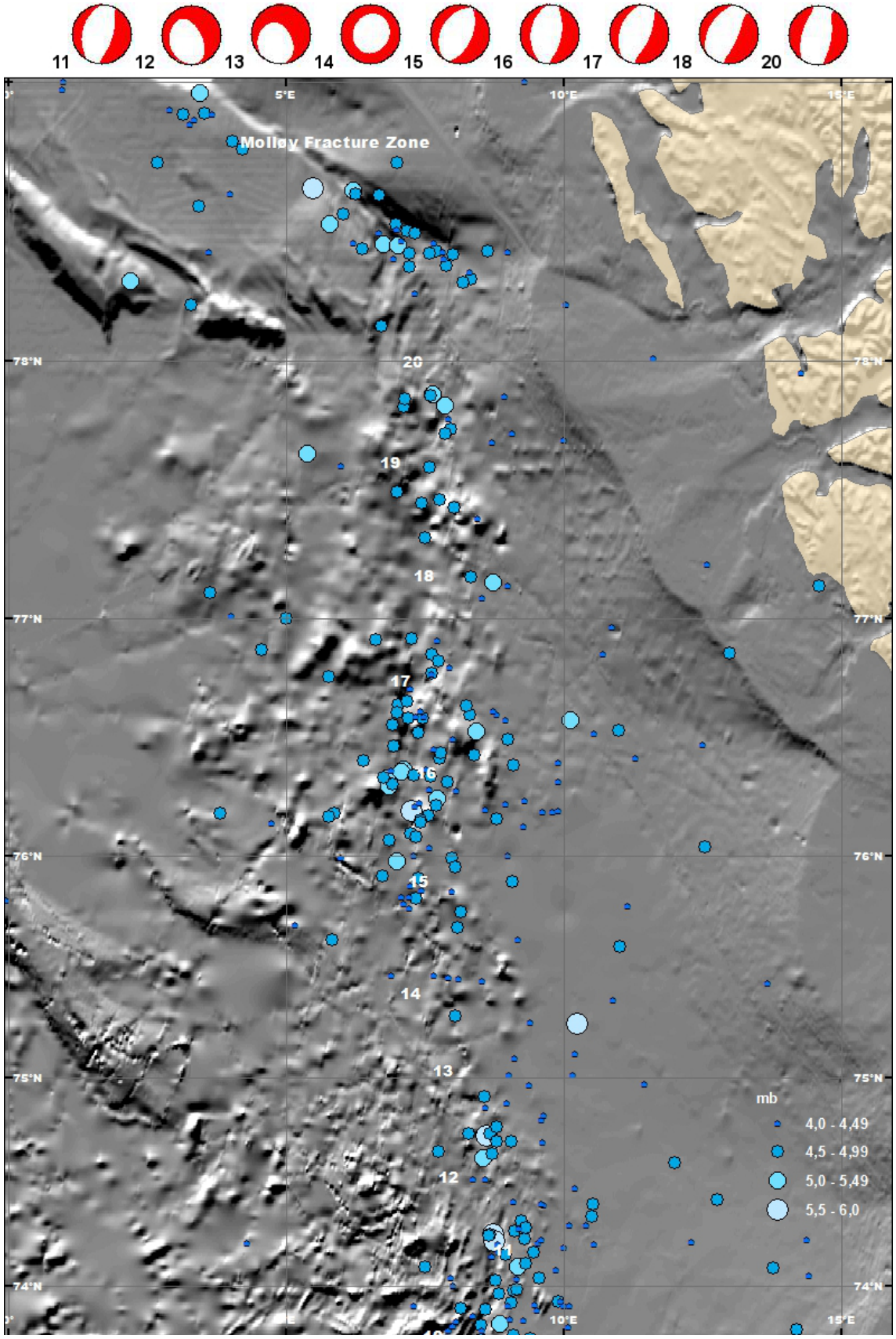

Figure 5.3: Overview map showing earthquake epicenters for all events with $m_b \geq 4.0$ around the Knipovich Ridge. Data were obtained from the International Seismological Centre's bulletin. Bathymetric map obtained from GEBCO. Map uses Mercator projection.

The diffuse nature of seismicity on the Knipovich Ridge is readily seen in figure 5.3. Large earthquakes are clustered in a few of the regions. From the map, regions 11, 12, 15, 16, and 20 (see table 8.1 in Appendix B for region/segment coordinates) seem more active than the rest. Normal fault plane solutions dominate here as well, mostly trending with the ridge axis. Region 16 stands out as clearly the most active, and a two of the fault plane solutions show reverse faulting (EventID 8030010, 11-1-06 and EventID 13786565, 19-9-09), which is unexpected. There is a zone of very little activity where the ridge meets the Molløy Fracture Zone, just as was seen for the Mohns Ridge. Four large earthquakes are located noticeably further from the ridge axis than the other big events, two on each side of the ridge. One of them is located on the Hovgård Ridge (approx. 78.29° N, 2.20°E) and may be linked to some activity there.

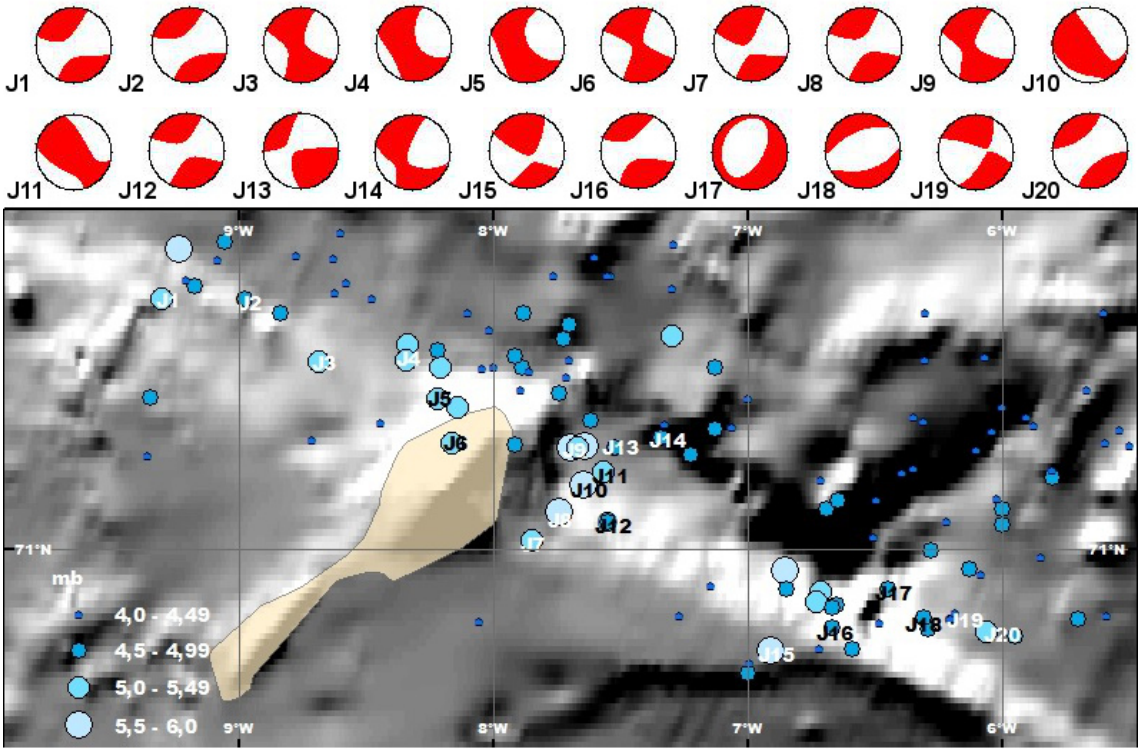

Figure 5.4: Overview map showing earthquake epicenters for all events with $m_b \geq 4.0$ on the Jan Mayen Fracture Zone. Data were obtained from the International Seismological Centre's bulletin. Bathymetric map obtained from GEBCO. Map uses Mercator projection.

The Jan Mayen Fracture Zone crosses the northern end of the island of Jan Mayen. Epicenters J4-J6 are located on the island itself, and many of the large earthquakes in this area are clustered around the flanks/shelf of the island. Most of the fault plane solutions show a strike-slip movement combined with a non-double-couple component, as is to be expected for a fracture zone. Two reverse fault plane solutions

are present, J11 and J12, on the eastern flank of the island. Only two clear normal faulting solutions are seen, J17 and J18, at the intersection of the fracture zone and the Mohns Ridge.

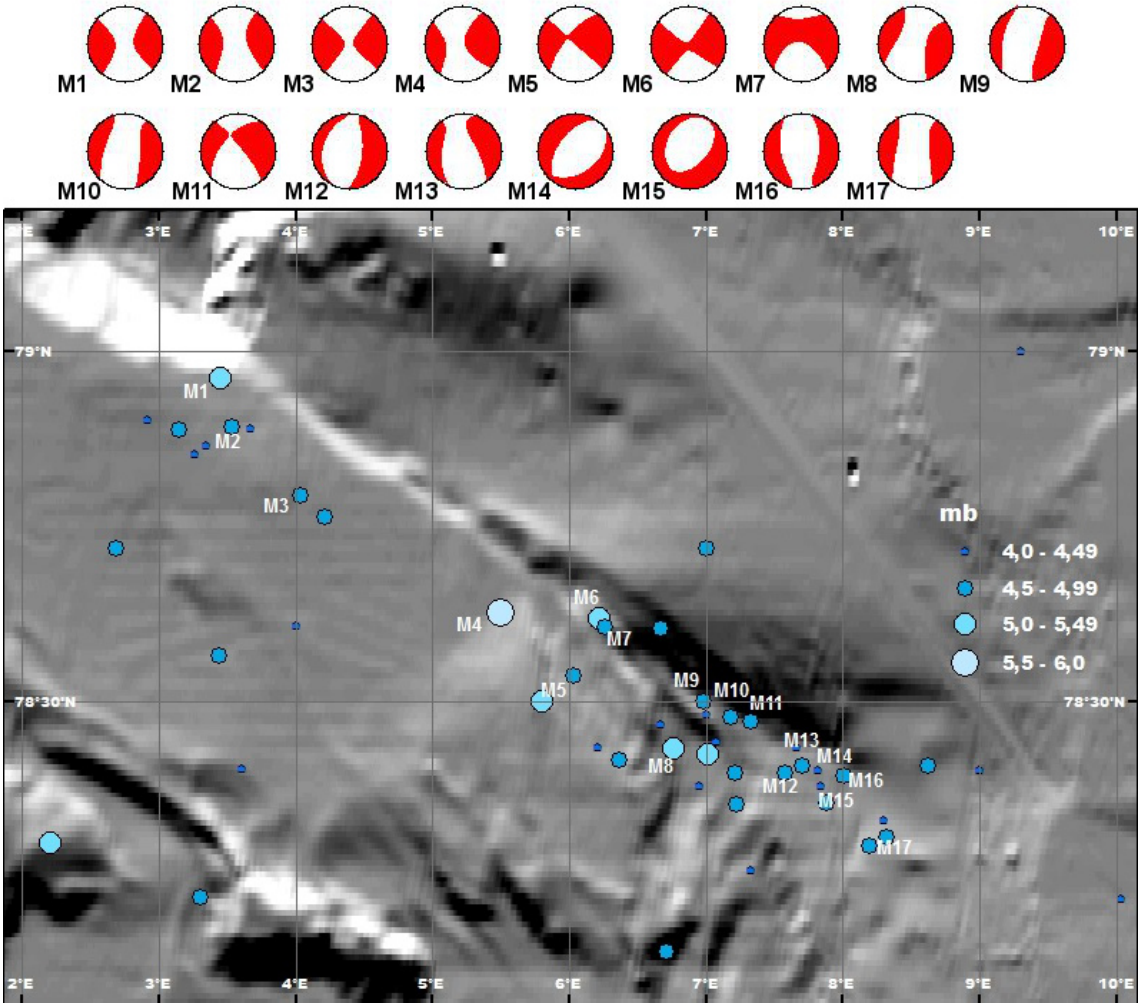

Figure 5.5: Overview map showing earthquake epicenters for all events with $m_b \geq 4.0$ on the Molløy Fracture Zone. Data were obtained from the International Seismological Centre's bulletin. Bathymetric map obtained from GEBCO. Map uses Mercator projection.

On the Molløy Fracture Zone, the seismicity is clearly split into two regions, and there is an approximately 30 km long gap where no earthquakes were recorded. Some of this may be attributed to the area's distance from seismogram networks, given that few earthquakes of magnitude $m_b \leq 4.5$ were present in the data. The single largest earthquake observed in this project was located at M4 on the map. The focal mechanisms for epicenters M1 through M8 all display strike-slip movement, at which point the mechanisms transition to normal faulting solutions (not including

M11) as they approach the intersection between the fracture zone and the Knipovich Ridge.

5.2 Largest seismic events

Several large earthquakes took place in the surveyed area during the time period of 1955-2015. 55 events had a moment magnitude $M_w \geq 5.0$, six of which reached a magnitude of 6.0 or greater. The single largest event had a moment magnitude of 6.6. It took place in July of 1992 at the Molløy Fracture Zone. The fault plane solution shows strike-slip faulting with non-double-couple component. Four out of the six largest events happened on the fracture zones, two on the Jan Mayen Fracture Zone and two on the Molløy Fracture Zone. These all display strike-slip faulting, as is to be expected. The last two took place on the Mohns Ridge, both displaying normal faulting. No exceptionally large intraplate earthquakes were found in the data. A few earthquakes with $m_b \geq 5.0$ were located further from the ridge axes, though none more than 100 km away.

Table 5.1: Largest earthquakes measured in the area from 1955-2015. Data and fault plane solutions from the International Seismological Centre.

EventID	M_W	m_b	Location	Date	Focal mechanism
283093	6.6	5.6	$78.63°N, 5.49°E$	20-07-1992	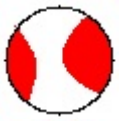
601033410	6.3	5.7	$73.03°N, 5.51°E$	24-05-2012	
15979160	6.2	6.0	$70.87°N, 6.91°W$	29-01-2011	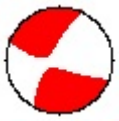
7489263	6.2	5.3	$78.61°N, 6.22°E$	02-05-2005	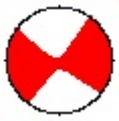
13588037	6.0	5.9	$72.21°N, 0.95°E$	20-08-2009	
1735664	6.0	5.3	$71.19°N, 8.22°W$	21-05-2000	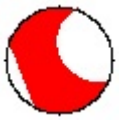

5.3 Earthquake sequences

Generally speaking, an earthquake sequence is a series of earthquakes closely spaced in both time and space. A sequence contains a mainshock clearly larger than the other shocks. A swarm is a series of earthquakes similar to a sequence but it has no mainshock. No large sequences were present in the data. Here, a sequence was defined as a series of at least five earthquakes taking place closely in space and time (less than 7 days between shocks). Using these criteria, a total of 19 sequences were found for the Mohns Ridge and three for the Knipovich Ridge. Six sequences had mainshocks on the Mohns Ridge, and one on the Knipovich Ridge. The largest sequence contained nine earthquakes and took place on the Mohns Ridge. The table below lists information about the five largest sequences.

Table 5.2: Largest earthquakes sequences measured in the area from 1955-2015. They are listed chronologically and the location, magnitude and fault plane solution are given for the largest quake in each sequence. Data and fault plane solutions from the International Seismological Centre.

First quake	Last quake	Location	Count	Largest quake [m_b]	Fault plane solution
07-08-74	08-08-74	$73.19°N, 6.30°E$	8	5.0	N/A
07-06-99	10-06-99	$73.02°N, 5.35°E$	9	5.2	
25-02-07	25-02-07	$73.18°N, 6.77°E$	8	5.1	
28-09-08	29-09-08	$71.26°N, 4.01°W$	9	5.2	
24-05-12	27-05-12	$73.03°N, 5.51°E$	8	5.7	

5.4 Gutenberg-Richter law

The Gutenberg-Richer law is an empirical law which expresses the relationship between the magnitude of an earthquake, M and the total number of earthquakes of that magnitude or higher, $N(M)$ for a given area and time period (Palacios, Molina, & Segovia, 2006). It is a simple logarithmic linear equation of the form:

$$log_{10}(N) = a - bM \tag{5.1}$$

where a and b are scaling parameters. While the a-value indicates the total seismicity rate of a region, the b-value is a power-law exponent of scaling. It describes how earthquake frequency decreases for each unit increase in magnitude. For example, in many seismically active regions, the b-value is close to 1.0 (Palacios et al., 2006). This means that for any given magnitude e.g. 6.0, there will be ten times as many earthquakes of magnitude 5.0 and 100 times as many of magnitude 4.0.
On a semilogarithmic graph of the frequency-magnitude distribution, the b-value is equal to the negative of the slope. The "roll-off" value M_{min} is an indicator of the sensitivity of the seismograph network. For a given M_{min}, the network has likely detected all earthquakes of that magnitude and higher. It should be noted that this number has not been constant throughout the time frame used here, the

value has likely decreased with increasing density of the seismograph network and improvements in technology (Utsu, 1965).

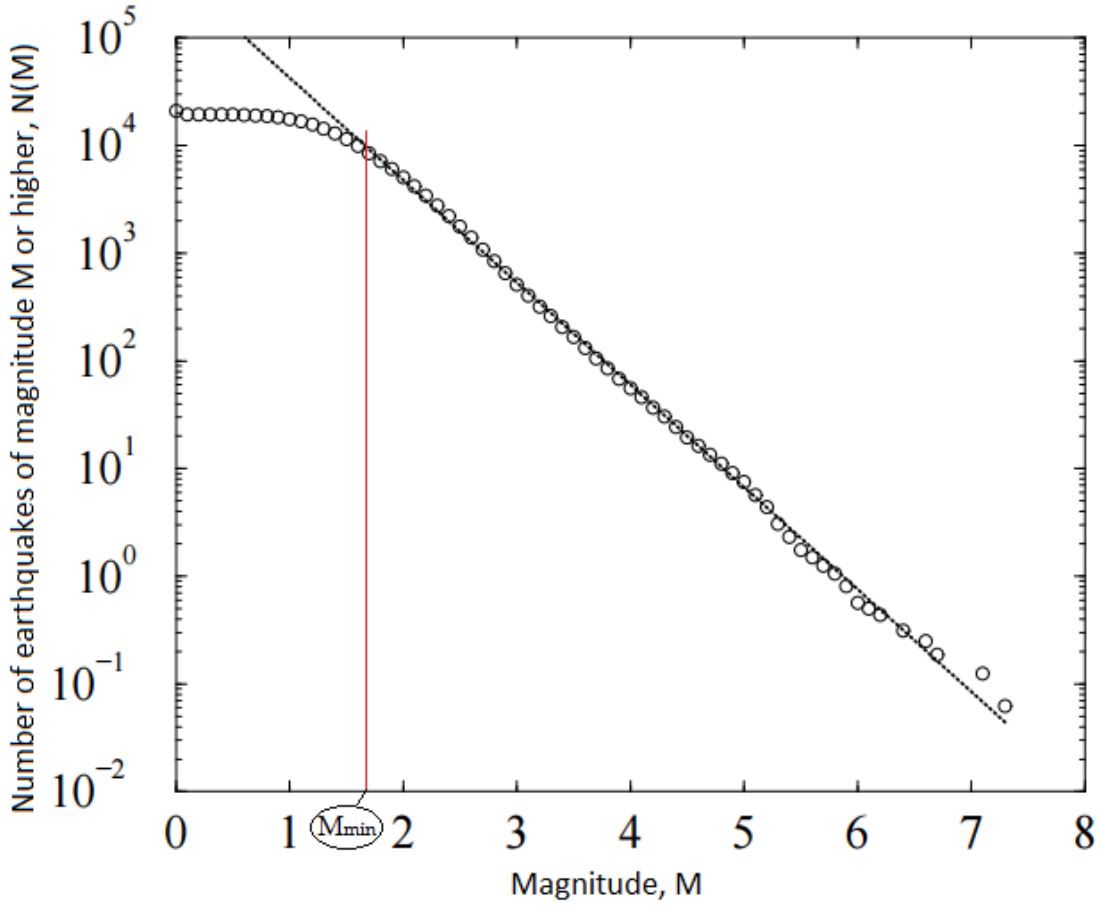

Figure 5.6: A semilogarithmic graph of the frequency-magnitude distribution. The slope of the dotted line is $-b$ and M_{Min} indicates the roll-off value (Bak et al., 2002).

Several methods can be used to determine the slope of the line. Three of the most common ones are estimating the slope by eye, the method of least squares, and the maximum likelihood method. The latter is best suited to this data set. That method uses the formula

$$b = \frac{log_{10}(e)}{M_{avg} - M_{min}} \tag{5.2}$$

where M_{avg} is the average magnitude of all recorded earthquakes with $M \geq M_{min}$.

The error for this method is estimated with:

$$e = \frac{b}{\sqrt{n}} \tag{5.3}$$

where n is the number of all recorded earthquakes with $M \geq M_{min}$.

The frequency-magnitude distribution was plotted for each ridge, both for the body-wave magnitude m_b and for the surface-wave magnitude M_s. Both types yielded very similar results, but the data contains far more of the m_b values and so the M_s plots are not included in this chapter.

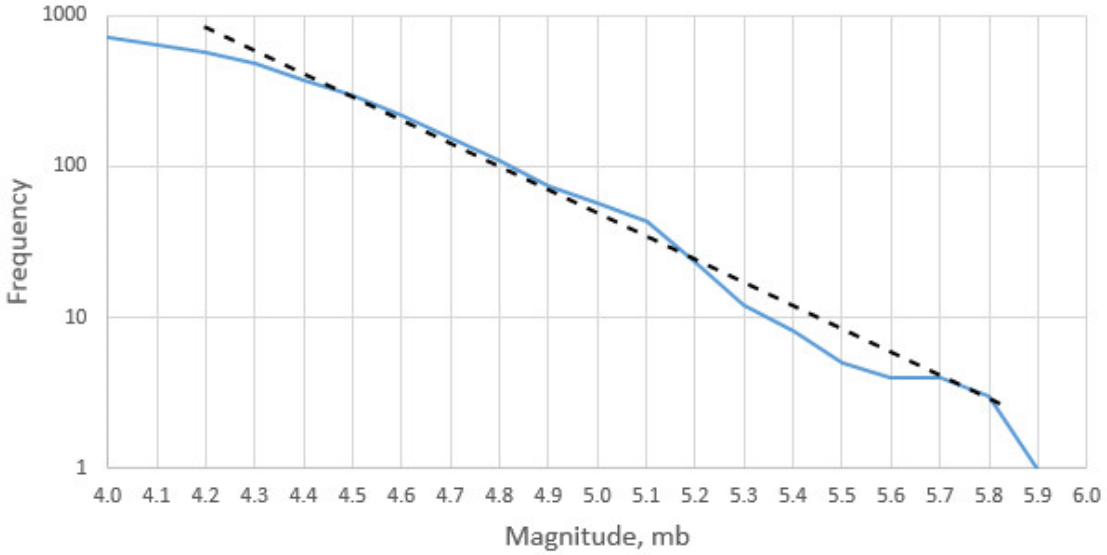

Figure 5.7: Mohns Ridge frequency-magnitude plot.

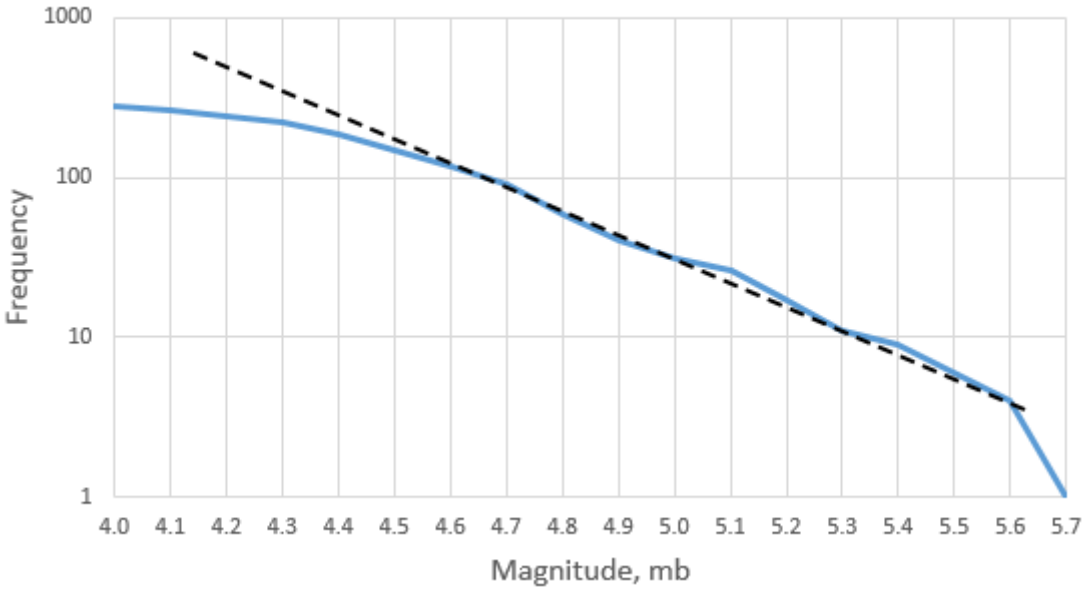

Figure 5.8: Knipovich Ridge frequency-magnitude plot.

Both plots exhibit good linearity, although the "trough" on the Mohns Ridge plot between magnitudes 5.2 and 5.7 may distort the calculation of the b-value. The dashed line is drawn in order to more clearly pinpoint where the linearity of each plot ends, i.e. where roll-off begins. The slope of this line should be close to the b-value for each region.
The roll-off value M_{min} can be difficult to determine from these plots, but it seems to lie between 4.4 and 4.5 for the Mohns Ridge and between 4.5 and 4.6 for the Knipovich Ridge. The table below lists the results when these values are used:

Table 5.3: Results from G-R calculations. The upper half lists results for Mohns Ridge and the lower for Knipovich Ridge.

M_{min}	M_{avg}	b	err	A
4.4	4.67	1.61	0.08	9.67
4.5	4.74	1.81	0.11	10.64
4.5	4.78	1.57	0.13	9.24
4.6	4.85	1.75	0.16	10.10

5.5 Seismic moment

The seismic moment is a quantity that measures the size of an earthquake based on the area of the fault **F**, average displacement during rupture $\underline{\mathbf{u}}$, and the shear modulus of the rock μ. It is given by the relation

$$M_0 = \mu \underline{u} F. \tag{5.4}$$

It is a useful parameter to describe the size of an earthquake, as it has a direct physical connection (Fowler, 1990). There is an empirical connection between the seismic moment M_0 and the moment magnitude of an earthquake M_w:

$$M_w = \frac{2}{3} log_{10}(M_0) - 6.0 \tag{5.5}$$

This method is obviously preferred when one has access to M_w measurements (Hanks & Kanamori, 1979).

M_W measurements were only available for a small portion of the seismic events used in this project (12%). m_b was plotted as a function of M_w and the two were found to have a relatively good correlation for $m_b \geq 4.0$:

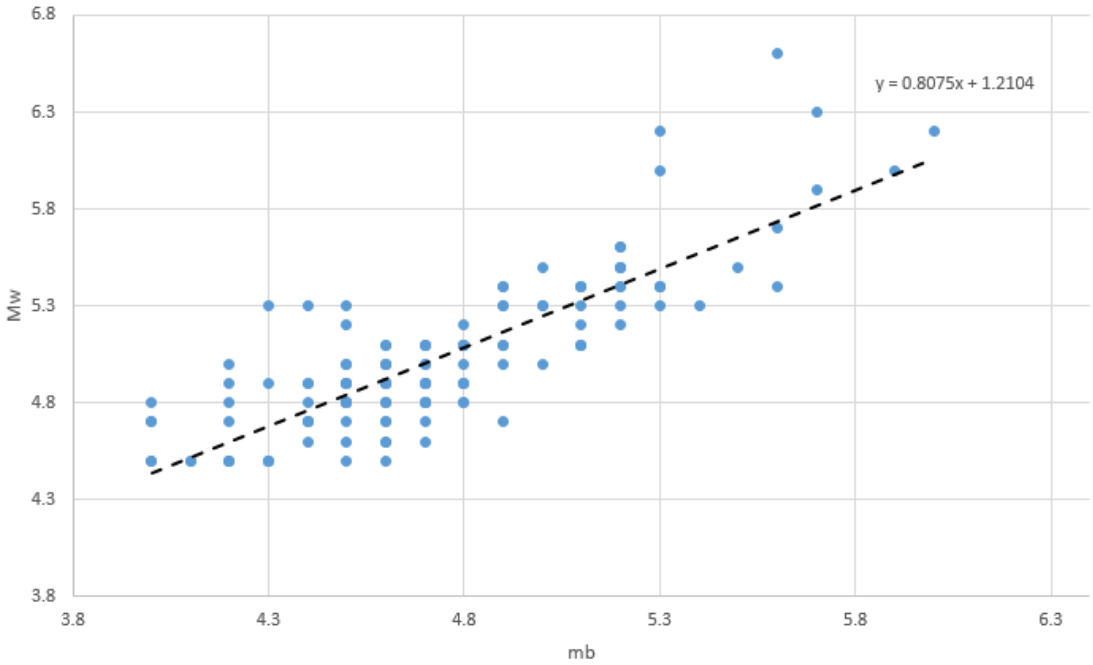

Figure 5.9: $m_b \geq 4.0$ as a function of M_W, note the correlation of 0.8075.

So in order to calculate the seismic moment for as many earthquakes as possible, a small adjustment was made to equation 3.5, i.e. m_b was used in place of M_w.
M_0 was then calculated for events on each ridge, with the ridges divided into segments. Longitudinal restrictions were applied in order to limit the data to include only events located at or near the ridge axes. Additionally, a few earthquakes had to be filtered out manually due to their distance from the ridges. For the Mohns Ridge, longitude was constrained between 5.686°W and 10.05°E, and for the Knipovich Ridge between 3.18°E and 12.78°E. The total seismic moment was calculated for each region. Since the ridges were not perfectly split into equally long segments, the length of a ridge present in each region was measured, and the total moment for a given region was divided by that length. The seismic moment was also calculated for the two fracture zones using the same method.

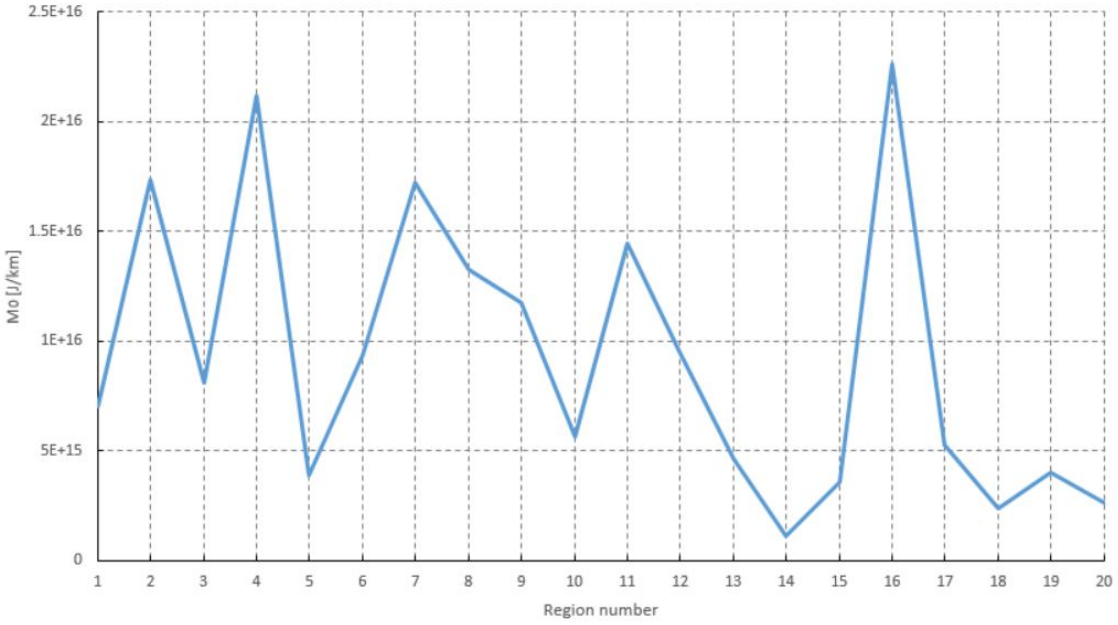

Figure 5.10: Normalized seismic moment for the both ridges. Regions 1-10 cover the Mohns Ridge and 11-20 the Knipovich Ridge.

No clear trend can be seen for the moment on the Mohns Ridge. It fluctuates along the length of the ridge, with three high peaks and low valleys. On the Knipovich Ridge, the moment drops noticeably from the south to the north, aside from a very large spike in region 16. It is unclear what causes this massive increase in activity. The Jan Mayen Fracture Zone was calculated as having normalized seismic moment of $M_0 = 3.55 \times 10^{16}$ J/km and the Molløy Fracture Zone $M_0 = 5.84 \times 10^{15}$ J/km. The contrast between the two is stark. While the Jan Mayen Fracture Zone has the highest moment, the Molløy Fracture Zone is on par with the lows on the Knipovich Ridge.

5.6 Spreading rate

For a divergent plate boundary, the spreading rate expresses how quickly the tectonic plates move away from one another. The half-spreading rate indicates how quickly one plate moves away from the spreading axis. Several methods can be used to measure or calculate these rates. The NUVEL-1A model of relative plate motion is a simple tool that can be used to calculate the spreading rate at a given point on a plate boundary. The calculations are derived from the trigonometry of a rigid, spherical triangle rotating around a fixed rotation pole on a sphere. Several variables are needed in order to perform the calculation and they are described in the table

below. The latitude is positive in the north direction, longitude is positive in the east direction, and the azimuth is clockwise positive, measured from the north (Barth et al., 2008).

Table 5.4: Variables used in calculating plate rotation

λ_p	Latitude of rotation pole
ϕ_p	Longitude of rotation pole
λ_x	Latitude of point on plate boundary
ϕ_x	Longitude of point on plate boundary
v	Amplitude of velocity on plate boundary
β	Azimuth of velocity on plate boundary
R	Radius of Earth
ω	Angular velocity about rotation pole

In order to properly describe the plate motion, we need to find both the amplitude and azimuth of the velocity vector. These can be calculated using the following formulas:

$$v = \omega R \sin a \tag{5.6}$$

$$\beta = 90^\circ + C \tag{5.7}$$

Since ω and R are known, we only need to find a and C. After some trigonometric gymnastics, we get the following equations:

$$a = \arccos[\sin(\lambda_x)\sin(\lambda_p) + \cos(\lambda_x)\cos(\lambda_p)\cos(\phi_p - \phi_x)] \tag{5.8}$$

$$C = \arcsin\left(\frac{cos(\lambda_p)\sin(\phi_p - \phi_x)}{\sin(a)}\right) \tag{5.9}$$

According to the model, the pole of relative rotation between the North American and Eurasian plates is located at $\lambda_p = 62.4^\circ N$, $\phi_p = 135.8^\circ E$, in northern Siberia. The angular velocity is given as $\omega = 0.22^\circ/Ma$. The speed and azimuth were calculated for several points along the ridge axes, spaced 0.5° latitudinally from one another. The amplitude of the velocity ranged from 16.9 mm/yr at the northern

end of the Knipovich Ridge to 14.4 mm/yr near the Jan Mayen Fracture Zone. The azimuth ranged from 128.3° to 114.7° between these points. These values line up well with current measurements of spreading rate (Mosar, Lewis, & Torsvik, 2002; Snow & Edmonds, 2007).

Table 5.5: Results from relative plate motion calculations

Latitude [°]	Longitude [°]	Amplitude [mm/yr]	Azimuth [°]
71.30	-5.63	16.91	114.7
71.80	-2.47	16.64	117.0
72.30	0.92	16.35	119.5
72.80	4.06	16.05	121.8
73.30	6.64	15.78	123.9
73.80	8.32	15.56	125.4
74.30	8.71	15.40	126.0
74.80	8.33	15.29	126.1
75.30	7.97	15.17	126.2
75.80	7.56	15.06	126.3
76.30	7.40	14.93	126.6
76.80	7.54	14.79	127.1
77.30	7.60	14.65	127.5
77.80	7.50	14.52	127.8
78.30	7.50	14.38	128.3

6 Conclusions

This thesis gives an overview of the seismic activity that has taken place on and around the Mohns Ridge and Knipovich Ridge during the period between 1955 and 2015. The results are mostly consistent with previous research in this area. A summary of the findings is provided below:

1) The Mohns Ridge is much more active than the Knipovich Ridge, as is to be expected. Seismic activity on the Mohns Ridge closely follows the ridge's axis, while activity is much more diffuse on the Knipovich Ridge. Fewer intraplate earthquakes are observed to the west of the ridges than to the east.

2) The fault plane solutions observed on the Mohns Ridge are all normal in nature and they largely line up with the trend of the ridge's axis. The Knipovich Ridge is dominated by normal fault plane solutions, most of which have some type of double-couple component. They do not follow the ridge axis's trend as closely.

3) A gap in seismicity is observed where the ridges connect to their respective fracture zones. The reason for this gap is unknown.

4) Fault plane solutions on both fracture zones are varied, displaying strike-slip and normal faulting. There is a large gap of no seismic activity on the Molløy Fracture Zone and a small one on the Jan Mayen Fracture Zone.

5) Four of the largest six earthquakes observed took place on the fracture zones, the final two taking place on the Mohns Ridge. Few noteworthy swarms were found in the data.

6) Area 16 on the Knipovich Ridge contains some anomalous findings; it has the highest normalized seismic moment of any ridge segment as well as reverse fault plane solutions. These observations are very interesting but it is beyond the scope

of this thesis to speculate about potential causes.

7) The calculated Gutenerg-Richter b-values of 1.61-1.81 for the Mohns Ridge and 1.57-1.75 for the Knipovich Ridge are close to expected values for mid-oceanic ridges.

8) The Mohns Ridge shows no clear trend regarding the seismic moment. On the Knipovich Ridge, the moment decreases from the south to the north, aside from the large spike in segment 16.

9) The calculated spreading velocity ranges from 16.9 mm/yr at the southern end of the Mohns Ridge to 14.4 mm/yr at the northern end of the Knipovich Ridge.

10) Activity on the Mohns Ridge is typical for a mid-oceanic ridge; earthquakes take place near the ridge's axis and all fault plane solutions display normal faulting. The seismic moment seems to show no clear trend. The Mohns Ridge is a less typical spreading ridge, earthquakes and thus deformation take place over a large area, with the precise location of the axis difficult to determine. Most of the fault plane solutions are in line with spreading ridge behavior and, aside from one anomalous region, the seismic moment drops to the north.

References

Bak, P., Christensen, K., Danon, L., & Scanlon, T. (2002). Unified scaling law for earthquakes. *Physical Review Letters*, *88*(17), 178501.

Barth, A., Reinecker, J., & Heidbach, O. (2008). Stress derivation from earthquake focal mechanisms [Journal Article]. *World Stress Map Project e Guidelines*, 12.

Cronin, V. (2004). A draft primer on focal mechanism solutions for geologists [Journal Article]. *Universidad de Baylor, Texas-EE. UU.< http://serc. carleton. edu/files/NAGTWorkshops/structure*, *4*.

Dauteuil, O., & Brun, J.-P. (1996). Deformation partitioning in a slow spreading ridge undergoing oblique extension: Mohns ridge, norwegian sea. *Tectonics*, *15*(4), 870–884. Retrieved from `http://dx.doi.org/10.1029/95TC03682` doi: 10.1029/95TC03682

Einarsson, P. (1986). Seismicity along the eastern margin of the north american plate. *The Geology of North America*, *1000*, 99–116.

Fowler, C. M. R. (1990). *The solid earth: an introduction to global geophysics* [Book]. Cambridge University Press.

GEBCO. (n.d.). *Gridded bathymetry data* [Web Page]. Retrieved from `http://www.gebco.net/data_and_products/gridded_bathymetry_data/`

Hanks, T. C., & Kanamori, H. (1979). A moment magnitude scale. *Journal of Geophysical Research: Solid Earth*, *84*(B5), 2348–2350. Retrieved from `http://dx.doi.org/10.1029/JB084iB05p02348` doi: 10.1029/JB084iB05p02348

ISC. (2015). *Isc bulletin* [Web Page]. Retrieved from `http://isc-mirror.iris.washington.edu/iscbulletin/search/bulletin/`

Kandilarov, A., Mjelde, R., Okino, K., & Murai, Y. (2008). Crustal structure of the ultra-slow spreading knipovich ridge, north atlantic, along a presumed amagmatic portion of oceanic crustal formation [Journal Article]. *Marine Geophysical Researches*, *29*(2), 109-134. doi: 10.1007/s11001-008-9050-0

Mosar, J., Lewis, G., & Torsvik, T. (2002). North atlantic sea-floor spreading rates: implications for the tertiary development of inversion structures of the norwegian–greenland sea. *Journal of the Geological Society*, *159*(5), 503–515.

Norton, M. (2008a). *Focal mechanism 01* [Figure]. Wikipedia. Retrieved from `https://en.wikipedia.org/wiki/File:Focal_mechanism_01.jpg`

Norton, M. (2008b). *Focal mechanism 02* [Figure]. Wikipedia. Retrieved from `https://en.wikipedia.org/wiki/Focal_mechanism#/media/File:Focal_mechanism_02.jpg`

Okino, K., Curewitz, D., Asada, M., Tamaki, K., Vogt, P., & Crane, K. (2002). Preliminary analysis of the knipovich ridge segmentation: influence of focused magmatism and ridge obliquity on an ultraslow spreading system. *Earth and Planetary Science Letters*, *202*(2), 275 - 288. Retrieved from `http://www.sciencedirect.com/science/article/pii/S0012821X02007902` doi: http://dx.doi.org/10.1016/S0012-821X(02)00790-2

Palacios, P., Molina, I., & Segovia, M. (2006). The gutenberg–richter law: assumptions, limitations and interpretations [Journal Article]. *Statistics in Volcanology. Special Publications of IAVCEI*, *1*, 115-127.

Snow, J. E., & Edmonds, H. N. (2007). Ultraslow-spreading ridges: rapid paradigm changes. *OCEANOGRAPHY-WASHINGTON DC-OCEANOGRAPHY SOCIETY-*, *20*(1), 90.

USGS. (1996). *Fault types* [Figure]. Author. Retrieved from `http://eqseis.geosc.psu.edu/~cammon/HTML/Classes/IntroQuakes/Notes/faults.html`

Utsu, T. (1965). A method for determining the value of b in a formula log n= a-bm showing the magnitude-frequency relation for earthquakes [Journal Article]. *Geophys. Bull. Hokkaido Univ*, *13*(99), 103.

7 Appendix A

Table 7.1 contains all relevant information about fault plane solutions in the dataset.

Table 7.1: Information about all earthquakes with fault plane solutions present in the dataset. Search parameters are listed in table 4.1. Data from the International Seismological Centre's bulletin.

EventID	Date	Lat	Long	m_b	mw	Strike/dip/rake	P Az/Pl	T Az/Pl	N Az/Pl	Author
13283717	06-12-07	71.331	-9.34	5.1	5.4	109/76/-7	65/14	333/5	224/74	NEIC
604090202	04-03-14	71.22	-8.89	4.5	5	108/82/-4	64/9	333/3	224/81	GCMT
1735724	24-05-00	71.12	-8.51	5.2	5.4	114/82/-7	69/10	339/1	244/80	HRVD
1058542	13-12-97	71.26	-9.34	5.2	5.6	104/64/-8	64/24	329/12	213/63	HRVD
1735664	21-05-00	71.08	-9	5.3	6	110/75/-27	66/29	161/8	264/60	HRVD
655921	08-12-95	72.28	3.28	5.4		14/40/-141	206/56	318/14	57/30	HRVD
13788743	22-06-09	76.29	6.44	5.2	5.6	14/51/-93	266/84	106/6	16/2	GCMT
7330023	14-04-04	71.067	-7.747	5.7	5.9	31/77/-175	254/13	346/5	97/76	NEIC
417897	08-12-95	72.28	3.28	5.6		14/40/-141	206/56	318/14	57/30	HRVD
6941267	19-06-03	71.122	-7.577	5.6	5.4	138/36/119	27/12	151/69	293/17	NEIC
7365085	14-05-04	71.849	-1.523	5.3	5.4	29/57/-100	268/76	127/11	35/9	ZUR_RMT
340095	08-12-95	72.28	3.28	5		14/40/-141	206/56	318/14	57/30	HRVD
533878	08-12-95	72.28	3.28	4.9		14/40/-141	206/56	318/14	57/30	HRVD
1735762	25-05-00	71.201	-7.332	4.7	5.1	106/57/-12	70/31	330/15	218/55	ZUR_RMT
15979160	29-01-11	70.96	-6.9	6	6.2	26/85/-150	254/25	156/17	35/60	NEIC
14322971	22-02-10	70.89	-6.64	4.9	5.3	113/84/-12	68/13	159/5	268/76	GCMT
13439079	22-06-09	76.29	6.44	4.7	4.9	14/51/-93	266/84	106/6	16/2	GCMT
1954476	19-07-01	70.979	-6.338	4.5	4.9	77/44/-81	82/83	340/1	250/7	ZUR_RMT
12789618	20-03-07	72.16	0.86	5.2	5.5	20/70/-122	252/54	134/19	32/30	GCMT
1755380	11-08-00	70.966	-6.372	4.3	4.5	26/66/-165	246/27	339/7	82/62	ZUR_RMT
161355	22-08-94	71.26	-6.35	5.3	5.3	190/90/-180	55/0	145/0	180/90	hrvd
6621789	26-03-03	71.401	-4.726	4.3	4.5	60/57/-98	304/77	156/11	65/7	ZUR_RMT
10699885	13-08-06	71.45	-4.05	4.8	5	24/55/-100	260/77	122/9	30/8	HRVD
13395402	28-09-08	71.4	-3.15	4.8	4.8	65/49/-77	34/80	146/3	236/9	NEIC
13395449	29-09-08	71.34	-4.35	4.7	4.8	106/87/-6	61/6	151/2	256/83	GCMT
401584	08-12-95	72.28	3.28	5.4		14/40/-141	206/56	318/14	57/30	HRVD
13229628	20-03-07	72.16	0.86	4.4	4.9	20/70/-122	252/54	134/19	32/30	GCMT
10699888	13-08-06	71.38	-4.06	4.2	4.7	59/61/-67	12/66	133/13	227/20	HRVD
1083379	23-03-98	71.54	-5.24	5.2	5.3	39/68/-96	298/67	134/23	42/6	HRVD
604583661	14-05-14	71.58	-3.36	3.9	4.8	26/56/-124	238/62	139/5	47/28	GCMT
3485792	12-10-02	71.572	-3.094	4.7	4.9	43/60/-109	274/69	147/13	53/16	ZUR_RMT
600668628	17-02-12	71.74	-2.29	4.6	5	29/51/-104	243/78	128/5	37/10	GCMT
605184096	31-08-14	71.66	-2.79	3.8	4.8	15/54/-111	231/71	120/7	28/17	GCMT
605184098	31-08-14	71.57	-2.89	3.8	4.6	52/62/-71	358/67	127/15	222/17	GCMT
13867450	19-10-09	71.59	-2.88	4.5	4.8	43/54/-82	346/79	127/9	218/7	GCMT
1055796	02-12-97	71.63	-2	5	5.3	14/15/-94	110/60	287/30	18/1	HRVD
1655494	13-04-99	73.21	6.65	5.1	5.2	63/31/-32	59/53	291/25	189/26	HRVD
605645287	04-11-14	71.86	-1.39	4.2	4.9	30/50/-101	245/81	128/4	38/8	GCMT
2051756	17-08-01	71.749	-2.631	4.6	4.7	40/60/-92	304/75	131/14	41/2	ZUR_RMT
7176164	04-11-03	71.791	-1.484	4.2	4.4	41/66/-98	296/68	137/20	45/7	ZUR_RMT
10698329	09-05-06	71.78	-7.01	4.5	4.6	96/46/97	180/0	86/85	270/5	HRVD
2051752	17-08-01	71.814	-2.542	4.6	4.6	34/66/-96	293/69	128/21	36/5	ZUR_RMT
7176460	05-11-03	71.8	-2.078	4.4	4.7	37/63/-94	299/71	129/18	38/3	ZUR_RMT

7 Appendix A

EventID	Date	Lat	Long	m_b	mw	Strike/dip/rake	P Az/Pl	T Az/Pl	N Az/Pl	Author
698203	08-12-95	72.28	3.28	5.1		14/40/-141	206/56	318/14	57/30	HRVD
3443452	28-09-02	71.847	-1.847	4.4	4.9	39/61/-95	296/74	132/15	41/4	ZUR_RMT
7491908	13-08-05	79.45	3.67	4.1	4.5	28/54/-71	350/73	104/7	196/15	HRVD
518589	08-12-95	72.28	3.28	5		14/40/-141	206/56	318/14	57/30	HRVD
561991	08-12-95	72.28	3.28	5.2		14/40/-141	206/56	318/14	57/30	HRVD
7553484	30-08-05	71.84	-1.23	4.8	5.1	41/55/-86	327/80	128/10	219/3	HRVD
605127878	01-08-14	72.01	-0.27	3.9	4.7	46/49/-85	355/85	133/4	223/4	GCMT
15089787	16-08-10	71.82	-1.46	4.7	5	39/61/-100	286/72	137/16	44/9	GCMT
601867059	01-11-12	71.95	-0.52	4.5	4.8	58/51/-71	30/75	134/4	225/15	GCMT
7342970	14-05-04	71.849	-1.523	4.4	4.7	29/57/-100	268/76	127/11	35/9	ZUR_RMT
15667126	18-11-10	72.22	0.38	4	4.8	19/47/-116	216/71	307/1	37/19	GCMT
689432	08-12-95	72.28	3.28	4.6		14/40/-141	206/56	318/14	57/30	HRVD
10701217	02-11-06	72.31	1.01	4.6	5	13/50/-117	215/70	122/1	31/20	GCMT
10699672	30-07-06	72.19	0.834	4.9	5.3	49/43/-68	49/74	304/4	213/15	NEIC
219256	12-07-93	72.64	0.56	5	5.3	9/69/-123	239/53	124/18	23/31	HRVD
11700491	20-03-07	72.16	0.86	4.5	4.9	20/70/-122	252/54	134/19	32/30	GCMT
13588037	22-06-09	76.29	6.44	5.9	6	14/51/-93	266/84	106/6	16/2	GCMT
10701219	02-11-06	72.14	0.75	4.5	4.9	52/58/-70	5/70	128/11	222/17	GCMT
386045	08-12-95	72.28	3.28	5		14/40/-141	206/56	318/14	57/30	HRVD
386049	08-12-95	72.28	3.28	5.1		14/40/-141	206/56	318/14	57/30	HRVD
7382123	22-07-04	78.483	7.96	4.6	4.8	9/52/-118	218/68	119/4	27/22	ZUR_RMT
1654948	13-04-99	73.21	6.65	4.9	5.4	63/31/-32	59/53	291/25	189/26	HRVD
2331828	08-11-01	72.395	2.236	4.9	4.7	27/39/-87	99/84	295/6	205/2	ZUR_RMT
7162593	20-10-03	72.479	3.223	4.2	4.3	40/72/-89	312/63	129/27	220/1	ZUR_RMT
601721529	17-09-12	72.46	2.6	4.5	4.8	22/60/-106	257/70	124/14	30/14	GCMT
2051704	16-08-01	72.618	2.707	4.7	4.9	26/55/-80	331/77	109/10	201/8	ZUR_RMT
1910841	01-02-01	73.481	7.855	4.6	5	46/60/-84	331/74	131/15	223/5	ZUR_RMT
1748045	25-05-00	71.201	-7.332	3.6	4.2	106/57/-12	70/31	330/15	218/55	ZUR_RMT
1748048	25-05-00	71.201	-7.332	4.2	4.5	106/57/-12	70/31	330/15	218/55	ZUR_RMT
62274	08-12-95	72.28	3.28	5.2	5.5	14/40/-141	206/56	318/14	57/30	HRVD
17000555	24-08-11	72.66	3.54	5.3	5.4	35/52/-100	263/80	132/7	41/8	GCMT
1728748	15-02-00	72.75	5.139	3.5	4.2	44/55/-72	2/72	121/9	214/15	ZUR_RMT
2429100	12-12-01	72.646	4.835	4.3	4.9	62/62/-72	7/68	139/15	233/15	ZUR_RMT
324680	08-12-95	72.28	3.28	5.4		14/40/-141	206/56	318/14	57/30	HRVD
601033774	25-05-12	72.99	5.47	4.8	5.2	36/53/-94	287/81	129/8	39/3	GCMT
1665454	07-06-99	72.68	4.36	5.2	5.5	6/63/-130	226/53	123/9	27/35	HRVD
601033410	24-05-12	73.08	5.71	5.7	6.3	53/43/-71	53/77	309/3	219/13	NEIC
1917183	01-02-01	73.481	7.855	4.7	4.6	46/60/-84	331/74	131/15	223/5	ZUR_RMT
1665458	26-08-99	71.68	-2.34	5	5.5	24/46/-102	212/82	122/0	32/8	HRVD
584706	08-12-95	72.28	3.28	5.2		14/40/-141	206/56	318/14	57/30	HRVD
3220642	08-04-02	73.832	7.93	4.8	4.8	37/45/-82	30/84	121/0	211/6	ZUR_RMT
604498552	28-04-14	73.22	6.61	4	4.7	35/60/-103	275/72	134/14	41/11	GCMT
11510030	25-02-07	73.26	6.76	5.1	5.4	30/51/-105	244/77	131/5	40/12	GCMT
1623138	13-04-99	73.21	6.65	4.7	5.1	63/31/-32	59/53	291/25	189/26	HRVD
11510071	25-02-07	73.29	6.8	4.6	4.9	17/53/-119	226/67	128/4	36/23	GCMT
7073294	30-08-03	73.58	5.24	4.8	5.1	21/80/-101	279/53	120/35	23/10	HRVD
11509674	25-02-07	73.37	7.21	4.6	4.9	0/72/-109	243/59	105/25	6/18	GCMT
606589205	19-01-15	73.22	6.35	4.9	5.4	16/52/-105	234/77	116/6	25/12	GCMT
11509983	25-02-07	73.33	6.96	4.6	5.1	19/58/-106	250/72	120/12	27/13	GCMT
2418840	05-12-01	73.37	6.8	4.7	4.8	59/45/-90	180/90	149/0	59/0	HRVD
509883	08-12-95	72.28	3.28	4.8		14/40/-141	206/56	318/14	57/30	HRVD
1763839	01-02-01	73.481	7.855	4.1	4.4	46/60/-84	331/74	131/15	223/5	ZUR_RMT
14704304	16-05-10	73.37	7.17	5.1	5.1	40/50/-82	0/83	124/4	215/6	GCMT
14704306	16-05-10	73.37	7.17	4.9	5.1	40/50/-82	0/83	124/4	215/6	GCMT
14705144	16-05-10	73.65	7.86	4.7	4.9	2/64/-117	231/61	111/15	15/24	GCMT
1763833	02-09-00	72.561	4.096	4	4.5	31/59/-104	267/72	130/13	38/12	ZUR_RMT
14712415	20-05-10	73.41	7.37	4.2	4.8	33/58/-92	297/77	125/13	35/2	GCMT
601709216	11-09-12	73.47	7.91	4.6	4.8	28/59/-99	274/74	125/14	33/8	GCMT
604484951	26-04-14	73.5	7.96	4.5	5.2	49/61/-68	360/66	123/14	218/19	GCMT
1763837	02-09-00	72.561	4.096	4.6	4.6	31/59/-104	267/72	130/13	38/12	ZUR_RMT
13280442	01-12-07	73.58	8.07	3.8	4.8	13/67/-104	257/65	113/20	18/13	GCMT
2969807	08-04-02	73.832	7.93	4.2	4.5	37/45/-82	30/84	121/0	211/6	ZUR_RMT
3255159	05-05-02	73.677	8.649	3.6	4.3	10/36/-103	146/78	289/10	20/7	ZUR_RMT
13280517	01-12-07	73.63	7.96	4.5	4.9	11/60/-100	257/73	109/15	16/9	GCMT
2969805	08-04-02	73.76	8.545	4.4	4.7	30/55/-82	331/78	114/9	205/7	ZUR_RMT
603963686	16-01-14	73.81	8.26	4.7	5	35/48/-86	352/86	122/2	212/3	GCMT
7485778	27-03-05	73.924	8.742	4.1	4.5	208/54/-71	171/73	285/7	17/15	ZUR_RMT
562401	08-12-95	72.28	3.28	5.1		14/40/-141	206/56	318/14	57/30	HRVD
10699162	30-06-06	73.98	8.68	4.6	5.1	17/55/-89	292/79	106/10	196/1	HRVD
10698672	28-05-06	74.03	13.63	5	5	20/51/130	263/1	355/60	172/30	HRVD
370547	08-12-95	72.28	3.28	5.5		14/40/-141	206/56	318/14	57/30	HRVD
11694343	10-03-07	74.23	8.72	5.6	5.7	20/46/-88	332/88	109/1	199/1	GCMT

EventID	Date	Lat	Long	m_b	mw	Strike/dip/rake	P Az/Pl	T Az/Pl	N Az/Pl	Author
3528381	12-10-02	71.572	-3.094	3.9	4.1	43/60/-109	274/69	147/13	53/16	ZUR_RMT
350207	08-12-95	72.28	3.28	4.8		14/40/-141	206/56	318/14	57/30	HRVD
3369371	09-09-02	74.695	9.095	4.3	4.5	5/56/-88	283/78	93/11	184/2	ZUR_RMT
6533903	09-01-03	74.68	8.797	4.6	4.9	14/35/-100	140/78	291/10	22/6	ZUR_RMT
668098	08-12-95	72.28	3.28	4.9		14/40/-141	206/56	318/14	57/30	HRVD
603045435	03-06-13	74.95	8.6	4.5	4.8	192/30/-54	211/64	76/19	340/17	GCMT
2954000	09-02-02	75.277	7.791	4	4.5	207/59/-74	154/71	286/13	19/14	ZUR_RMT
2347411	16-11-01	74.72	8.08	4.9	5	216/37/-37	207/55	90/18	350/29	HRVD
1727743	03-02-00	75.16	9.45	5.5	5.5	212/41/142	87/14	198/55	348/32	HRVD
2891473	09-02-02	75.277	7.791	4.7	4.7	207/59/-74	154/71	286/13	19/14	ZUR_RMT
7417617	11-10-04	75.678	7.069	4.4	4.3	29/42/-86	80/86	296/3	206/2	ZUR_RMT
603265614	03-06-13	74.95	8.6	4.6	4.9	192/30/-54	211/64	76/19	340/17	GCMT
7417629	11-10-04	75.985	7.437	4.6	4.5	44/23/-77	110/67	304/22	212/5	ZUR_RMT
603860365	17-12-13	75.93	6.9	4.3	5.3	23/53/-95	269/81	116/8	26/4	GCMT
604007097	16-01-14	73.81	8.26	4.4	5.3	35/48/-86	352/86	122/2	212/3	GCMT
603874637	23-12-13	76.03	7.15	3.6	4.8	7/58/-116	227/66	115/9	22/22	GCMT
73714	04-10-95	75.87	6.24	5.1	5.3	220/32/-50	230/62	101/18	4/20	HRVD
513489	08-12-95	72.28	3.28	4.6		14/40/-141	206/56	318/14	57/30	HRVD
601792484	06-10-12	75.97	6.88	4.8	4.9	9/56/-102	244/76	107/10	15/10	GCMT
8030010	11-01-06	76.41	6.2	4.7	4.8	173/34/113	67/12	199/72	334/13	HRVD
7442517	27-11-04	76.18	7.16	4.9	5.1	10/54/-89	284/81	99/9	189/1	HRVD
272255	08-12-95	72.28	3.28	5.7		14/40/-141	206/56	318/14	57/30	HRVD
272407	08-12-95	72.28	3.28	5.2		14/40/-141	206/56	318/14	57/30	HRVD
13217739	20-03-07	72.16	0.86	5.1	5.1	20/70/-122	252/54	134/19	32/30	GCMT
14931608	20-05-10	73.41	7.37	5.3	5.4	33/58/-92	297/77	125/13	35/2	GCMT
13209641	20-03-07	72.16	0.86	4.6	4.7	20/70/-122	252/54	134/19	32/30	GCMT
2040973	19-07-01	70.979	-6.338	4.5	4.8	77/44/-81	82/83	340/1	250/7	ZUR_RMT
13202283	20-03-07	72.16	0.86	5.1	5.4	20/70/-122	252/54	134/19	32/30	GCMT
6697823	22-04-03	76.746	7.398	4.4	4.8	9/41/-111	181/75	294/6	26/14	ZUR_RMT
13786565	22-06-09	76.29	6.44	4.8	4.9	14/51/-93	266/84	106/6	16/2	GCMT
15051809	30-07-10	76.32	7.11	4.2	5	20/67/-91	288/68	111/22	21/1	GCMT
603762235	28-10-13	76.41	6.78	5.4	5.3	17/51/-103	232/79	116/5	25/10	GCMT
600332421	07-02-12	76.89	6.8	4.8	5.1	23/56/-87	303/78	111/11	202/2	GCMT
981772	20-08-96	78.07	6.95	5.2	5.2	2/48/-103	207/80	102/3	11/10	HRVD
113013	09-03-95	78.78	1.46	5.1	5.1	137/47/71	60/0	330/76	15/14	HRVD
318364	08-12-95	72.28	3.28	5.2		14/40/-141	206/56	318/14	57/30	HRVD
1802948	01-02-01	73.481	7.855	4	4.7	46/60/-84	331/74	131/15	223/5	ZUR_RMT
388898	08-12-95	72.28	3.28	5		14/40/-141	206/56	318/14	57/30	HRVD
283093	08-12-95	72.28	3.28	5.6	6.6	14/40/-141	206/56	318/14	57/30	HRVD
441540	08-12-95	72.28	3.28	4.9		14/40/-141	206/56	318/14	57/30	HRVD
7489263	13-08-05	79.45	3.67	5.3	6.2	28/54/-71	350/73	104/7	196/15	HRVD
7489189	02-04-05	78.63	6.497	4.5	5.3	221/66/-17	181/28	88/6	348/61	ZUR_RMT
601670454	02-09-12	78.42	6.59	5.2	5.4	241/64/-18	202/30	108/7	6/59	GCMT
209599	23-09-93	78.16	6.5	4.8	5.1	19/58/-83	309/76	104/13	195/6	HRVD
7374334	21-07-04	78.467	7.005	4.7	4.8	211/44/-59	201/69	100/4	8/21	ZUR_RMT
7489192	13-08-05	79.45	3.67	4.5	5	28/54/-71	350/73	104/7	196/15	HRVD
10698146	28-04-06	78.49	6.64	4.5	4.7	4/60/-99	251/74	100/14	9/8	HRVD
7374585	22-07-04	78.483	7.96	3.8	4.2	9/52/-118	218/68	119/4	27/22	ZUR_RMT
7064130	18-08-03	78.416	7.655	4.6	4.8	200/44/-44	185/58	79/10	344/30	ZUR_RMT
7185109	16-11-03	78.416	7.582	4.2	4.5	55/39/-74	79/78	314/7	223/10	ZUR_RMT
7245541	30-01-04	78.359	8.002	4.4	4.6	45/55/-74	360/74	124/9	216/13	ZUR_RMT
3153782	08-04-02	73.832	7.93	4.8	4.9	37/45/-82	30/84	121/0	211/6	ZUR_RMT
10699808	09-08-06	78.46	7.64	4.7	5.1	215/50/-43	190/55	94/5	1/34	HRVD

8 Appendix B

The table below lists how the ridges were divided into segments.

Table 8.1: Table listing ridge segmentation. No constraints were applied to longitude.

Segment	Bottom latitude [°N]	Top latitude [°N]
1	71.17	71.45
2	71.45	71.73
3	71.73	72.01
4	72.01	72.29
5	72.29	72.57
6	72.57	72.85
7	72.85	73.13
8	73.13	73.41
9	73.41	73.69
10	73.69	73.97
11	73.97	74.40
12	74.40	74.83
13	74.83	75.26
14	75.26	75.69
15	75.69	76.12
16	76.12	76.55
17	76.55	76.98
18	76.98	77.41
19	77.41	77.84
20	77.84	77.27